JMB

Available online at www.sciencedirect.com

SCIENCE *d* DIRECT°

ELSEVIER

Crystallographic Studies on Decameric *Brucella* spp. Lumazine Synthase: A Novel Quaternary Arrangement Evolved for a New Function?

Sebastián Klinke[1], Vanesa Zylberman[1], Daniel R. Vega[2] Beatriz G. Guimarães[3], Bradford C. Braden[4] and Fernando A. Goldbaum[1]*

[1]*Fundación Instituto Leloir C1405BWE Buenos Aires Argentina*

[2]*Comisión Nacional de Energía Atómica, B1650KNA Provincia de Buenos Aires, Argentina*

[3]*Laboratório Nacional de Luz Síncrotron, Caixa Postal 6192 CEP 13084-971 Campinas SP, Brazil*

[4]*Department of Natural Sciences, Bowie State University, Bowie, MD 20715-9465, USA*

*Corresponding author

The enzyme lumazine synthase (LS) catalyzes the penultimate step of riboflavin biosynthesis in plants, fungi and bacteria. The quaternary structure of the polypeptide differs between species, existing as pentamers or as icosahedrally arranged dodecamers of pentamers with 60 subunits. The pathogen *Brucella* spp. expresses two proteins that exhibit LS activity, RibH1 and RibH2. The latter enzyme belongs to a novel third category of quaternary arrangement for LS, that of a decameric structure assembled as a head-to-head oriented dimer of pentamers. In contrast, the RibH1 enzyme is assembled as a pentamer, as noted for several other LS enzymes. RibH1 appears to be the functional LS in *Brucella* spp., whereas RibH2, an enzyme of lower catalytic activity, is a virulence factor presumably acting in response to oxidative stress. The latter observation prompted us to further investigate the structural and catalytic properties of RibH2 in order to clarify the biological function of this enzyme. Here, we present a detailed analysis of two new crystallographic forms of RibH2 that explain the low catalytic activity of this enzyme in comparison with RibH1 and other LSs. Additionally, we analyze the effect of pH on the structure of this enzyme, and the binding of riboflavin and 6,7-dimethyl-8-ribityllumazine to its active site.

© 2005 Elsevier Ltd. All rights reserved.

Keywords: 6,7-dimethyl-8-ribityllumazine synthase; X-ray crystallography; riboflavin biosynthesis; quaternary arrangement; *Brucella* spp.

Introduction

Riboflavin (vitamin B2) is an essential cofactor for all living organisms. This compound is the precursor of flavin mononucleotide (FMN) and flavin adenine dinucleotide (FAD), two key coenzymes involved in redox processes in the cell. Plants, fungi and bacteria are able to synthesize riboflavin, whereas animals must acquire it through diet. This, along with the inability of certain micro-organisms to incorporate exogenous riboflavin,[1–3] identify the enzymes involved in riboflavin biosynthesis as promising targets of chemotherapeutic agents.[4]

The biosynthesis of riboflavin has been studied extensively.[5–9] Figure 1 highlights the terminal reactions of this process. The penultimate step is catalyzed by the enzyme 6,7-dimethyl-8-ribityllumazine synthase (LS), which facilitates the condensation of 5-amino-6-(D-ribitylamino)-2,4(1*H*,3*H*)-pyrimidinedione **1** with (3*S*)-3,4-dihydroxy-2-butanone-4-phosphate **2** to yield 6,7-dimethyl-8-ribityllumazine **3**. This compound then undergoes a dismutation reaction, catalyzed by the enzyme riboflavin synthase (RS), to yield riboflavin **4** with the regeneration of one molecule of **1** that
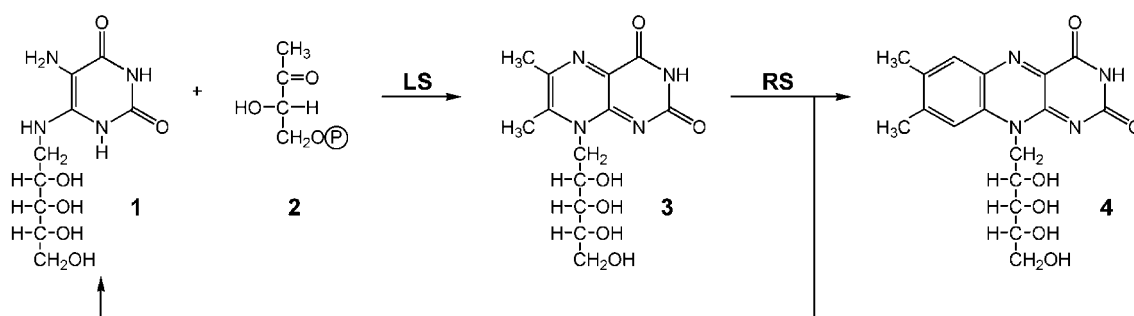
Figure 1. Terminal reactions in riboflavin biosynthesis. The enzymes involved are 6,7-dimethyl-8-ribityllumazine synthase (lumazine synthase, LS) and riboflavin synthase (RS).

serves as substrate for LS to start a new reaction cycle. From a stoichiometric point of view, one equivalent of **1** and two equivalents of **2** give rise to one equivalent of riboflavin **4**. A mechanism for the reaction catalyzed by LS has been proposed in terms of crystallographic, biochemical and spectroscopic analyses.[10–12]

To date, lumazine synthases (LSs) from eight different species have been described by X-ray crystallography. Although the building blocks of these enzymes are homopentamers in all cases, LS from spinach[13] and from the bacteria *Bacillus subtilis*[14–16] and *Aquifex aeolicus*[17] are dodecamers of pentamers, giving rise to icosahedral particles of about 1 MDa and exhibiting 532 symmetry. On the other hand, the fungus *Magnaporthe grisea*,[13] the bacterium *Mycobacterium tuberculosis*,[18] and the yeasts *Schizosaccharomyces pombe*[19] and *Saccharomyces cerevisiae*[20] express an LS whose polypeptide assembles only as pentamers.

Brucella spp., the infectious agent that causes the disease brucellosis, also expresses LS as part of its riboflavin biosynthetic pathway. The RibH2 protein of this microorganism, which shows LS activity,[21] was the first member described for this function and was thus assigned as the actual LS of this bacterium. However, we found recently that a second protein coded in the *Brucella* spp. genome, namely RibH1, also presents this enzymatic activity, but with an enhanced catalytic efficiency (V.Z. *et al.*, unpublished results). This observation prompted us

to further investigate the structural and enzymic properties of RibH2.

RibH2 has been used extensively as a serological marker for brucellosis, indicating that this protein is expressed at high levels during the host–bacterium interaction. The detection of antibodies specific for this protein antigen made it possible to differentiate active from inactive brucellosis.[22] In cattle, detection of antibodies to *Brucella* spp. RibH2 proved useful to distinguish between animals vaccinated with strain 19 of *Brucella abortus* and pregnant heifers infected experimentally with a virulent strain of *B. abortus*.[23] It is important to state that all sequenced *Brucella* species, namely *B. abortus*, *B. melitensis* and *B. suis*, share exactly the same RibH2 sequence.

In contrast to RibH1, which is assembled as a pentamer (V.Z. *et al.*, unpublished results), RibH2 presents a remarkable divergence in its quaternary arrangement in comparison with LS from other species.[24] Crystallographic and solution studies demonstrate that it assembles as a very stable decamer, which is best described as a head-to-head dimer of pentamers, giving rise to a third category of quaternary association for LSs. We have presented the crystallographic structure of RibH2 elsewhere.[24,25] Here, we present an extensive description of critical features of the enzyme *via* a detailed comparison with two new three-dimensional models of RibH2, one at different pH to show the influence of this variable in the structure, and the other with a bound substrate analogue inhibitor to this enzyme (Figure 2). We analyze how its novel quaternary arrangement results in a lower catalytic activity for RibH2 with respect to RibH1 and other LSs. In total, these differences lead to the hypothesis that RibH2 performs a different function in the cell although conserving LS activity.
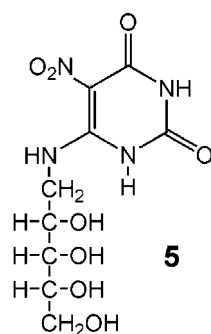
Results and Discussion

X-ray crystallographic structure analysis

We have crystallized and solved the structure of *Brucella* spp. RibH2 both in its free form at pH 6.5

Figure 2. Chemical structure of 5-nitro-6-(D-ribityl-amino)-2,4(1*H*,3*H*)-pyrimidinedione (NRP), a substrate analogue inhibitor of lumazine synthase.

(RibH2-ORTH) and in complex with the substrate analogue inhibitor 5-nitro-6-(D-ribitylamino)-2,4(1*H*,3*H*)-pyrimidinedione **5** at pH 6.3 (RibH2-NRP). The X-ray structures were solved by the molecular replacement method using the previously known structure of *Brucella* spp. RibH2 at pH 4.8 (RibH2-RHO; PDB code 1DI0) as search model.[25] RibH2-ORTH crystallizes in the orthorhombic space group $P2_12_12_1$ with a complete decamer in the asymmetric unit and diffracts to 3.05 Å. The crystals of RibH2-NRP diffract to a maximum resolution of 2.90 Å and belong to the trigonal space group $P3_121$, with a single pentamer in the asymmetric unit and a very high solvent content of about 71% (v/v). Symmetry operators of the space group generate the full decameric structure from the homopentamer. RibH2-NRP was refined to $R = 0.217$ and $R_{free} = 0.254$ with good stereochemistry. Ramachandran statistics of this structure showed that 95% of all residues lie in the most favorable regions, with the remaining 5% in additionally allowed zones. The first eight to ten N-terminal residues of each LS polypeptide present no electronic density due, presumably, to their enhanced mobility and therefore were excluded from the final model, as were the last one to four C-terminal residues of each chain. With the exception of these termini, the double difference Fourier map presents continuous density with no main-chain break. Only two exposed polar residues (Arg152 from chain A and Glu121b from chain B) present poor or missing side-chain electronic density and were modeled as alanine. The inhibitor molecule NRP is very well defined in the Fourier maps. A total of five phosphate anions were added to the model in the last stages of refinement. The RibH2-ORTH model was refined to $R = 0.199$ and $R_{free} = 0.256$ with acceptable geometry. In this case, 90.7% of the residues are inside the most favorable regions in the Ramachandran plot, with 9.1% in additionally allowed regions and 0.2% in generously allowed zones. There is no residue in a disallowed area. The final model corresponds to a decameric motif, which resembles the solution state of the enzyme. Both pentameric modules superimpose very well with a C^α root-mean-square deviation (r.m.s.d.) of 0.40 Å, a value that lies within the experimental error for the working resolution. As with the ligand-bound model, there is lack of electron density at both ends of the polypeptide chains in the RibH2-ORTH structure, but in this case the number of residues with deficient side-chain density increased to about 30 for the whole molecule, perhaps due to the lower resolution of this structure. The quality of the $2F_o - F_c$ Fourier map is consistent with the resolution, allowing for the precise identification of several solvent molecules and ion atoms. In both structures, the calculated self-rotation functions show a strong peak at κ near 72°, indicating the presence of 5-fold symmetry in the molecule. Despite the existence of non-crystallographic symmetry, both models were refined without restraints to the monomers. In this

Table 1. Refinement statistics for both structures solved in this work

	RibH2-NRP	RibH2-ORTH
Resolution limits (Å)	52.0–2.90	56.0–3.05
R-factor	0.217	0.199
Free *R*-factor	0.254	0.256
Non-hydrogen protein atoms	5739	11,360
Non-hydrogen ligand atoms	105	–
Solvent molecules	89	16
Non-hydrogen ion atoms	25	202
r.m.s.d. bond lengths (Å)	0.007	0.008
r.m.s.d. bond angles (deg.)	1.40	1.61
B-factor (average, Å²)	41.3	23.5

sense, superposition of individual chains leads to average C^α r.m.s.d. of only 0.27 Å for RibH2-NRP and 0.39 Å for RibH2-ORTH, supporting the observation that both models obey a strict pentameric architecture in each crystal form. Additionally, due to the fact that both C5 axes of each pentamer are coaxial in the decamer, the molecule belongs to the symmetry point group D5. Statistics of the refinement process are shown in Table 1.

RibH2 overall structure

The overall fold of the 18 kDa *Brucella* spp. RibH2 monomer has been described in detail.[25] Briefly, it is formed by a single domain composed of a central β sheet with four parallel strands ($\beta_3\beta_2\beta_4\beta_5$), surrounded by four helices, two on one side ($\alpha_2\alpha_3$) and two on the other ($\alpha_1\alpha_4$). This 158-residue monomer closely resembles that of *B. subtilis*, the first LS described.[14] As noted above, all known LSs share a common pentameric building block. However, some critical variations between *Brucella* spp. RibH2 and other LS sequences lead to striking differences in quaternary arrangement and catalytic properties that will be discussed later in this work.

In *Brucella* spp. RibH2, monomer–monomer contacts in the pentameric moiety bury about 35% of their solvent-accessible area, primarily through hydrophobic contacts. Pentamer formation is essential for catalytic activity, since the active site of the enzyme lies at the monomer–monomer interfaces involving residues from two neighboring chains.[14]

The presence of a single pentamer in the asymmetric unit of the first solved *Brucella* spp. RibH2 structure (RibH2-RHO) prompted us to perceive that this enzyme is a pentamer in solution.[25] However, crystallographic symmetry expansion of this structure and other mid-resolution forms of RibH2 always resulted in a particular head-to-head association of two pentamers, giving rise to a decameric assembly. Static light-scattering experiments corroborate this hypothesis, yielding a molecular mass of 180 kDa for the whole particle.[24] Additionally, we demonstrated in a previous work that for protein engineering purposes, the decameric assembly can be dissociated into pentamers and further regenerated using guanidinium chloride.[26] Both structures

solved in this work agree with those observations. Thus, *Brucella* spp. RibH2 is the first LS of known three-dimensional structure that is arranged as a dimer of pentamers. The basis for this unique quaternary arrangement lies in a short sequence of amino acid residues close to the C terminus.[20] In *B. subtilis* LS, there is a characteristic five-residue loop (GTKAG) connecting helices α4 and α5, and involved in pentamer–pentamer contacts stabilizing the icosahedral capsid. On the other hand, pentameric *S. cerevisiae* LS presents a longer loop comprising nine residues between these helices, making it unable, due to steric clashes, to assemble as an icosahedron. RibH2 also presents insertions in this part of the monomer but, unlike the other LS, these extra residues do not arrange as a loop but lead to the formation of an undistorted helix between α4 and α5 that we view as an extended α4 helix. In order to stabilize this 32-residue long helix (residues 122–153), its N terminus is further removed from the previous β5 sheet (residues 110–118) when compared to the pentameric and icosahedral LS.[25] This leads to a longer loop connecting the β5 and α4 elements, making residues 121–134 in *Brucella* spp. RibH2 essentially non-superposable with other LSs (Figure 3). Moreover, this region makes extensive
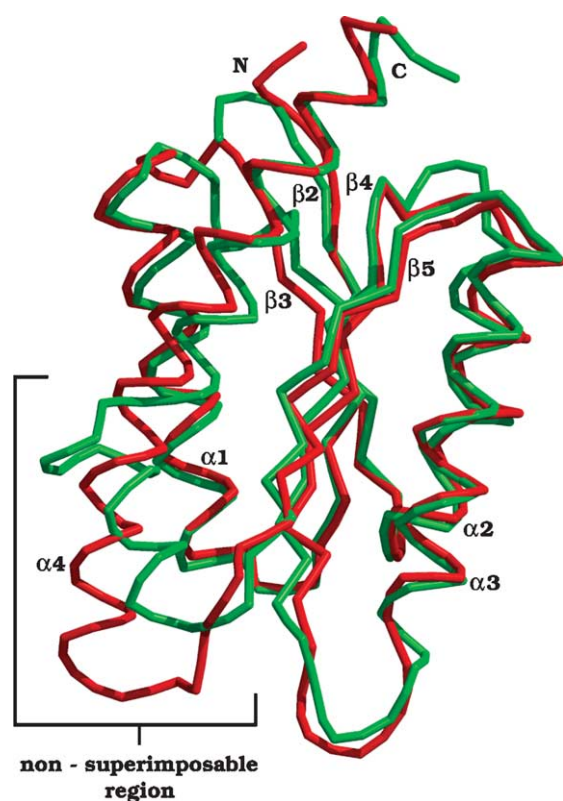
contacts with the neighboring pentamer in the decameric motif and presents a higher structural dependence on the environment pH, as will be discussed below. Thus, changes in a limited part of the monomer lead to this novel quaternary arrangement for the protein.

Binding of a substrate analogue inhibitor

The active site of *Brucella* spp. RibH2 is located at the interfaces between monomers and features a high degree of exposure to the solvent. A total of five segments are involved in its formation. Residues 21–23 (loop connecting β2 to α1), 55–58 (loop connecting β3 to α2), and 80–92 (C terminus of β4, N terminus of α3 and their bridging loop) account for almost the entire binding site. In addition, the active site cavity is complemented by residues from a neighboring chain, namely 131′, 135′ and 138′ from helix α4 and 113′–116′ from strand β5.

Figure 4 shows an overall view of the RibH2 structure in complex with the substrate analogue inhibitor NRP (RibH2-NRP). The ligand shows clear electron density in all binding sites in the crystal structure. Although the general folding of RibH2-NRP is conserved in comparison with the free RibH2-RHO structure, superposition of ligand-bound and free monomers (Figure 5) highlights a significant difference in two regions: residues 83–87 (region 1), a loop connecting β4 to α3, and residues 119–126 (region 2) involving the loop after strand β5 and the N terminus of helix α4. Although C^{α} r.m.s.d. for the entire monomer is 0.79 Å, this value rises to 1.88 Å and 1.63 Å, respectively, for these regions individually. The most striking observation is that these regions account for almost all pentamer–pentamer contacts. Moreover, a high number of these residues present different side-chain orientations between the native and ligand-bound structures. For example, in the RibH2-RHO structure, His120 contacts the same amino acid residue in the neighboring pentamer in a π–π stacking conformation, and performs a major side-chain rearrangement upon ligand binding to stack the previous residue, His119. Next, His121a, which interacts with Glu121b in the same chain in the free structure, turns about 90° to stack His121a from the neighboring pentamer in the RibH2-NRP structure. Additional changes in the complex are the displacement of about 2 Å of the main chain in region 1 (Asp83, Gly84 and Gly85) towards the pentamer–pentamer interface to make new contacts with His119, His121a and His124, and the rearrangement of Ser121c and Lys122 to interact with different amino acid residues in the same chain. All these changes lead to an altered interface, although conserving the same decameric quaternary arrangement. In addition, there are marked differences in the temperature factors of the C^{α} in these regions (Figure 6). RibH2-RHO presents an average *B*-factor of 42 Å^2 for each monomer; however, increasing to $B = 87 \text{ Å}^2$ and $B = 91 \text{ Å}^2$ for residues of regions 1 and

Figure 3. Superposition of monomers from decameric *Brucella* spp. (red) and icosahedral *A. aeolicus* LS (green). Secondary structure notations are shown close to each element. The presence of a single continuous helix at the C terminus of the *Brucella* spp. enzyme determines its unique quaternary structure.
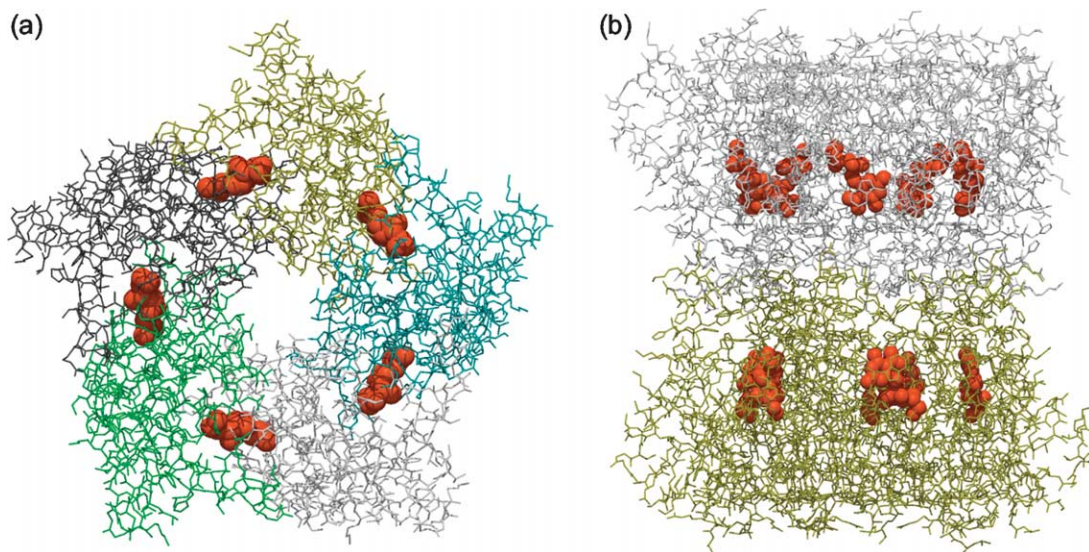
Figure 4. (a) Top view of the asymmetric unit of the complexed *Brucella* spp. RibH2-NRP structure. Every monomer is drawn in a different color, whereas the NRP molecules are presented as space-fill models in red. (b) Front view of the decameric biological assembly of this enzyme. The particle folds as a head-to-head dimer of pentamers (each of them depicted in a different color) to give rise to a spool-like structure.

2 alone. On the other hand, RibH2-NRP shows comparable thermal factors along the entire monomer ($B = 40$ Å^2), with no appreciable change

Figure 5. Superposition of monomers of free RibH2-RHO (black) and complexed RibH2-NRP (yellow). Significant differences were found in both marked regions.

at the conflicting regions ($B = 34$ Å^2 for region 1 and $B = 42$ Å^2 for region 2). In summary, RibH2-NRP presents quite a different pentamer–pentamer interface with increased rigidity in comparison to the free RibH2-RHO structure. This observation agrees with the increased number of van der Waals and salt-bridge contacts seen in the enzyme interface when a substrate analogue is bound.
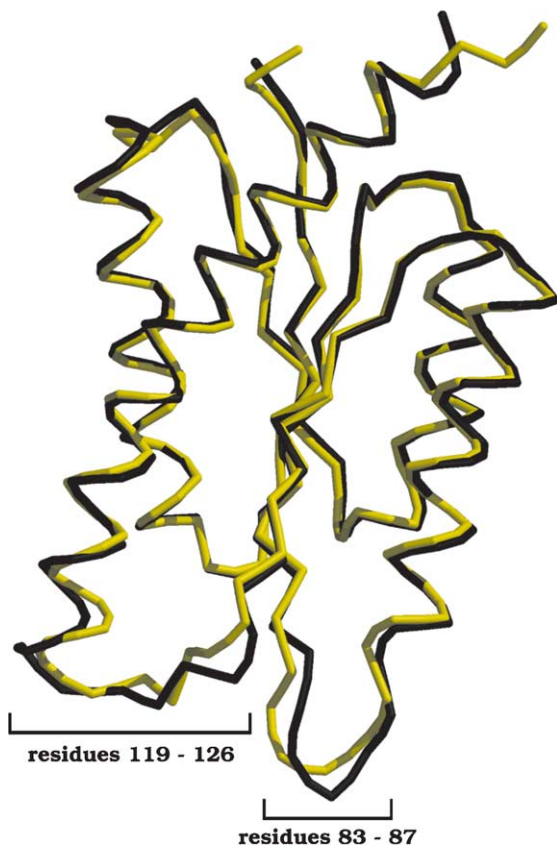
Reasons for the variability at the pentamer–pentamer interface

The significant structural differences observed between RibH2-RHO and RibH2-NRP at the equatorial pentamer–pentamer interface may be the consequence of several factors, including substrate analogue inhibitor binding and the different crystallization conditions for both proteins, concerning mainly space group and mother liquor pH. To clarify, we performed an extensive analysis of every possible source of divergence. RibH2-NRP was crystallized in the $P3_121$ space group using 0.1 M Mes (pH 6.5), 30% (w/v) PEG 400, 0.1 M sodium acetate, with a final mother liquor pH of 6.3. In contrast, RibH2-RHO crystals grew in the rhombohedral *R*32 space group with 1.25 M ammonium sulfate in 0.1 M sodium phosphate buffer (pH 5.0), having a final pH of 4.8.[25] The differences in space group can be discarded as a source of variation at the pentamer–pentamer interface, as we know that the enzyme is a dimer of pentamers, and although the full molecule is constructed by applying crystallographic symmetry to single pentamers in both structures, the residues at the pentamer–pentamer interface are not involved in contacts between molecules, the usual cause of side-chain and main-chain shifts in X-ray
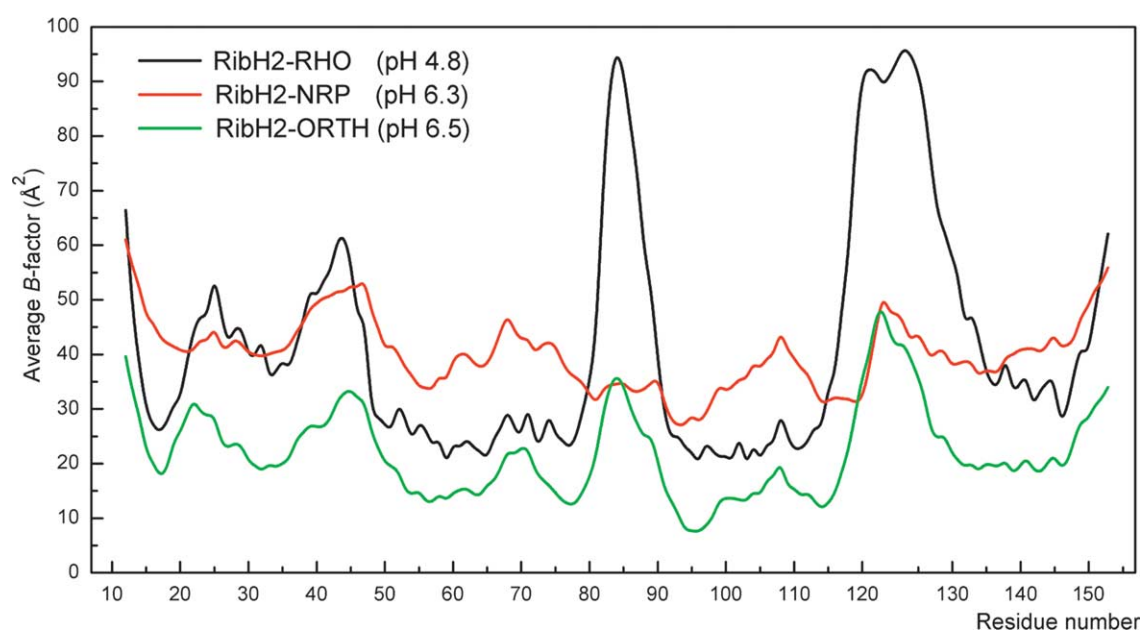
Figure 6. Comparison of C$^\alpha$ *B*-factors of the previously solved RibH2 structure and the two new RibH2 models presented here. The larger separation found between residues 120 and 125 is due to the presence of the amino acid residues 121a, 121b and 121c in the sequence, which were identified originally in this way in order to preserve the numbering of the superposable residues at the end of the C-terminal helix with those of *B. subtilis* LS.

models. The only visible change caused by the distinct space groups is a different packing of the dimers of pentamers in the crystals. In addition, we did not find any evidence that could prove a direct influence of ligand binding on the modification of the pentamer–pentamer interface. As can be seen in Figure 4(b), the location of the NRP molecules in the enzyme is not far removed from the interface. However, the shortest distance between the ligand and the residues contacting the neighboring pentamer is about 9 Å, from the nitro group of NRP to the main chain of Gly85. There is no direct contact with the conflicting residues, nor any sign of conformational change upon binding that could result indirectly in such a significant modification of the interface.

Provided that space group differences and ligand binding could be rejected from our analysis, we focused on the influence of pH. *Brucella* spp. RibH2 includes an unusually high number of histidine residues at the interface region, comprising seven amino acid residues of a stretch of 16 from His119 to His131 (Figure 7). In the RibH2-NRP structure, solved at pH 6.3, five of these His residues contact the neighboring pentamer, including van de Waals and salt-bridge contacts, as well as π-π stackings between the imidazole moieties of two histidine residues, namely His119 from pentamer A, His120 from pentamer B (ten interactions per decamer) and His121a with the same residue in the neighboring pentamer (five per decamer). It is known that histidine residues become protonated at pH values below 6.0, leading to charge repulsions and subsequent loss of non-covalent bonds. This is apparent for the RibH2-RHO structure solved at

pH 4.8, where their interface histidine residues are involved in fewer contacts than in the RibH2-NRP structure, losing, for example, the His119-His120 stacking. Accordingly, RibH2 dissociates in solution into intermediate pentamers at pH below 5.0, as shown by static light-scattering studies,[24] again indicating the influence of pH on the structure of the protein. This analysis supports the conclusion that the alteration at the interface is a consequence of the pH differences and not of the substrate analogue binding. To corroborate this hypothesis, we solved the structure of free RibH2 at pH 6.5
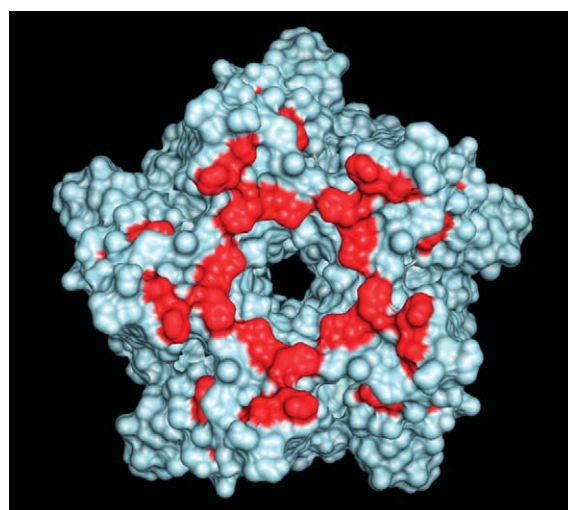

Figure 7. Histidine residues (red) at the pentamer–pentamer interface. They comprise the amino acid residues 119, 120, 121a, 124, 125, 129 and 131.

Table 2. C^α root-mean-square deviation values (in Å) obtained after superposition of monomers from RibH2-RHO, RibH2-NRP and RibH2-ORTH

Structures superimposed	RibH2-ORTH (pH 6.5)	RibH2-NRP (pH 6.3)
RibH2-RHO (pH 4.8)	0.74	0.79
RibH2-NRP (pH 6.3)	0.35	–

(RibH2-ORTH) and performed an exhaustive comparison of the pentamer–pentamer interface with the free structure at pH 4.8 and the complexed form at pH 6.3. We found that RibH2-ORTH and RibH2-NRP present a very similar interface, each making the same kind of contacts and having similar side-chain orientations for the conflicting residues. Furthermore, both structures near pH 6.5 present a higher C^α r.m.s.d. with respect to RibH2-RHO, as shown in Table 2. In addition, interface *B*-factors of RibH2-ORTH resembled those of the RibH2-NRP structure, with an average value of 22 Å^2 over each monomer and local values of 32 Å^2 and 40 Å^2 for regions 1 and 2, respectively. Figure 6 clearly shows the contrast of the RibH2-RHO structure in terms of the thermal factors, demonstrating how the fewer and lower-quality contacts lead to a more flexible, i.e. enhanced mobility, interface. In conclusion, all of these observations agree that pH plays a critical role in the structure of the interface between pentamers in *Brucella* spp. RibH2.

Molecular recognition of the bound NRP ligand

As previously noted, the substrate analogue inhibitor NRP binds tightly to the active site of the RibH2 enzyme, due to its minor differences with the natural substrate **1**. This ligand is recognized by means of several well-defined hydrophilic and hydrophobic contacts, involving residues from two neighboring subunits within a pentamer. Figure 8 shows the main hydrophilic contacts. Briefly, two oxygen atoms and a nitrogen atom of the pyrimidine ring of NRP are hydrogen bonded to complementary main-chain atoms of the protein, and the four ribityl oxygen atoms are hydrogen bonded with ε oxygen atoms of the highly conserved residue Glu58 or with main-chain amide and carbonyl groups of the enzyme. Bonding distances are presented in Table 3. Recognition is complemented by hydrophobic interactions with both sides of the pyrimidine ring. These comprise a non-polar region generated by side-chains of Val81, Val82 and Ala56 at one face, and a strong stacking with the indole group of Trp22 at the other face (Figure 9). This latter interaction forms a coplanar π complex with a separation of about 3.5 Å, and plays a central role in substrate recognition and catalysis. In almost all known LS sequences, either tryptophan or phenylalanine is present at this position, signifying the importance of this interaction. Superposition of RibH2-NRP and RibH2-RHO structures shows that Trp22 undergoes a side-chain rearrangement upon ligand binding in order to achieve proper stacking. Moreover, the electron density of Trp22 in the complexed RibH2-NRP enzyme is well defined in contrast with both free RibH2-RHO and RibH2-ORTH models. It is important to note that
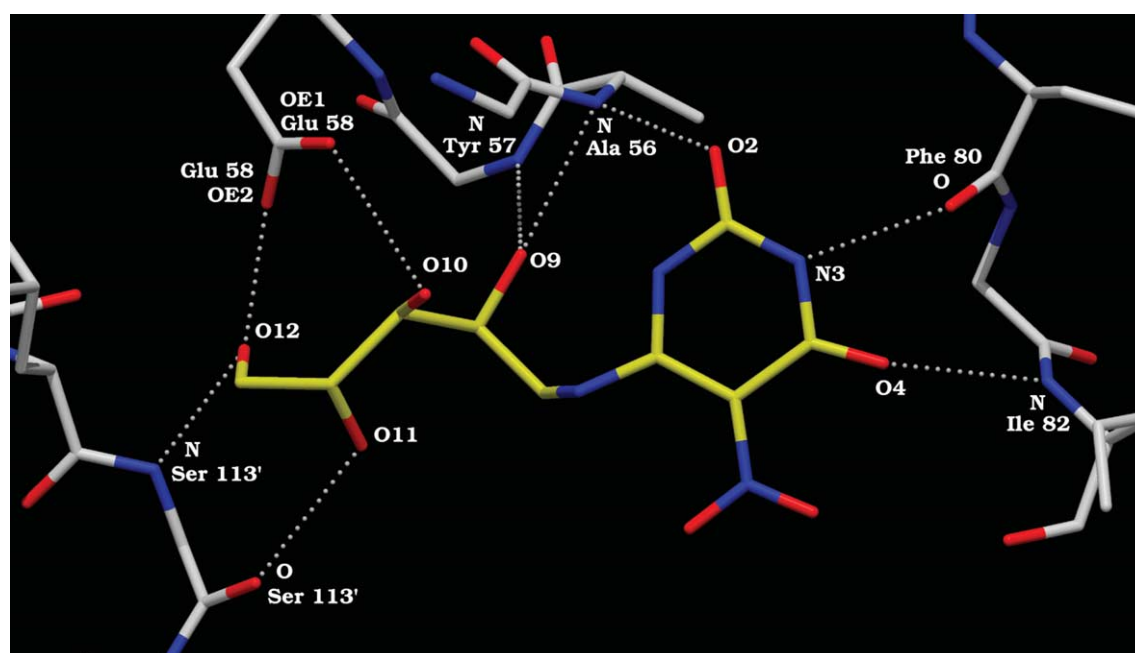

Figure 8. Hydrophilic contacts involved in the recognition of the NRP ligand.

Table 3. Average distances between ligand and enzyme atoms involved in hydrophilic contacts

Ligand atom	Enzyme atom	Distance (Å)
O2	Ala56 N	2.79
N3	Phe80 O	2.80
O4	Ile82 N	2.91
O9	Ala56 N	2.88
O9	Tyr57 N	2.86
O10	Glu58 OE1	3.25
O11	Ser113′ O	2.93
O12	Glu58 OE2	2.54
O12	Ser113′ N	2.89

the contacts and binding site of NRP in *Brucella* spp. RibH2 are superimposable to other known LS bound to the same or structural related ligands,[11,13,16,18–20] as this region of the active site is highly conserved between species. In contrast, the (3S)-3,4-dihydroxy-2-butanone-4-phosphate **2** binding site of *Brucella* spp. RibH2 presents remarkable differences with respect to other LS, as will be discussed below.

Role of bound phosphate in the active site

The RibH2-NRP crystallization conditions contain an appreciable amount of phosphate. In the final cycles of refinement, strong spherical electron density was found in each of the active sites approximately 6 Å from the NRP molecule. These peaks were subsequently modeled as bound phosphate ions. These ions are bound to the four backbone amide groups of residues 84–87 and the protonated NE2 nitrogen atom of His119. Phosphate groups were observed in other LS structures when present in the crystallization solutions. It has been proposed that this bound ion and the phosphate group of the substrate (3S)-3,4-dihydroxy-2-butanone-4-phosphate **2** share the same binding site in the protein.[15] Unfortunately, compound **2** is highly unstable[10] and, consequently, there is no related LS complex known to date to fully describe its recognition by the enzyme. None-

theless, it is clear that the residues that contact these phosphate groups are not the same in RibH2 compared with other LS. This observation leads to proposed differences in the catalytic properties of the *Brucella* spp. RibH2, as discussed below.

Binding of 6,7-dimethyl-8-ribityllumazine and riboflavin

We found that RibH2 binds to the inhibitor NRP ($K_D = 0.042$ μM), to the usual product of the LS catalysis (6,7-dimethyl-8-ribityllumazine, $K_D = 1.0$ μM) and to the final product of the biosynthetic pathway, riboflavin ($K_D = 7.5$ μM) (V.Z. *et al.*, unpublished results). As these molecules share a high level of structural homology, especially at the ribityl side-chain and the pyrimidinedione moiety (see Figures 1 and 2), it is expected they bind in a manner similar to that of the natural substrate 5-amino-6-(D-ribitylamino)-2,4(1*H*,3*H*)-pyrimidine-dione. Moreover, the binding of riboflavin to RibH2 is strongly competed by NRP, demonstrating clearly that all these molecules bind to the same site in the enzyme (V.Z. *et al.*, unpublished results). When 6,7-dimethyl-8-ribityllumazine and riboflavin are modeled in the active site of the RibH2-NRP structure, it is observed that both molecules fit well in this cavity with no steric clash (Figure 10).

To date, only one structure of LS bound with riboflavin has been described, that of the yeast *Schizosaccharomyces pombe* enzyme.[19] Unfortunately, all attempts to obtain X-ray-quality, high-diffracting crystals of *Brucella* spp. RibH2 bound with riboflavin have been unsuccessful. However, valuable information can be extracted from the modeled structure. For the *S. pombe* enzyme, the aromatic rings of riboflavin are recognized by means of two
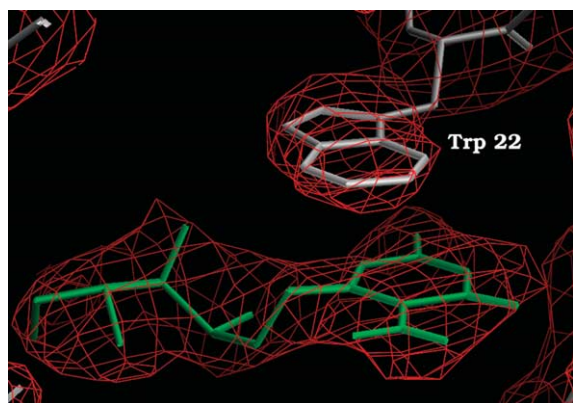
Figure 9. Offset stacking interaction between the pyrimidine ring of NRP and Trp22. The final $2F_o - F_c$ electronic density map is shown at the 1.4 σ level.
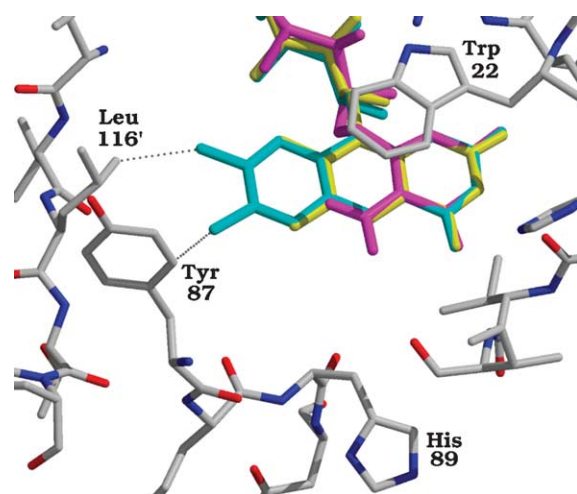
Figure 10. Putative binding of riboflavin (light blue) and 6,7-dimethyl-8-ribityllumazine (yellow) to the active site of the RibH2-NRP structure. The bound NRP molecule is drawn in pink. Hypothetical contacts between the xylene methyl groups and two side-chains of the protein are shown as dotted lines (distances of about 3 Å each).

stacking interactions: Trp27 (Trp22 in *Brucella* spp.) parallel with the pyrimidine ring, and residue His94 (His89 in *Brucella* spp.) located on the opposite side of riboflavin linked to its xylene ring. These strong stacking interactions are dominant in the K_D of 1.2 μM for riboflavin. On the other hand, the RibH2 model shows that only the stacking with Trp22 would be present in the complex. As shown in Figure 10, His89 points in a different orientation, precluding any interaction with the xylene ring of riboflavin, even after side-chain torsion. The lack of this interaction would lead to a much higher value of K_D; however, we find only a slightly increased dissociation constant (7.5 μM). This result can be interpreted by the potential two extra contacts formed between the methyl groups of the riboflavin and the residues Tyr87 and Leu116′, which are absent from the *S. pombe* enzyme.

Influence of the quaternary arrangement on the catalytic activity

As noted previously, *Brucella* spp. RibH2 presents a decameric quaternary structure that differs from all other described LS. This special arrangement leads to significant effects on the catalytic properties of the enzyme. Although the binding mode of NRP is highly conserved among species, there are marked differences in the recognition of substrate **2**, mainly at its phosphate group. For example, all known pentameric and icosahedral LS bind this phosphate by means of a salt-bridge involving the well-conserved Arg127 residue (Figure 11(a)). This is the last residue of the α4 helix and is located immediately before the above-mentioned loop that establishes the quaternary structure of the protein. In contrast, the *Brucella* spp. enzyme presents a completely different secondary and tertiary structure at this position, due to the presence of the undistorted and longer α4 helix at the end of the

polypeptide chain (see Figure 3: superposition of the monomers from *Brucella* spp. RibH2 and the icosahedral *A. aeolicus* LS). The equivalent residue to Arg127 in the *Brucella* spp. sequence, namely His124, is about 3 Å away in the opposite direction of the active site from its equivalent position in the *A. aeolicus* structure. This variation in the polypeptide chain leads to the absence of a positively charged group able to contact the phosphate group of molecule **2** in the *Brucella* spp. enzyme, as shown in the RibH2-NRP structure. The only positive amino acid residue in the vicinity of this ion is His119, which is about 4 Å away (Figure 11(b)). This distance is more than 1 Å longer than that observed between Arg127 and the phosphate group in other species, thus leading to a weaker interaction with the ion. Moreover, the average *B*-factor of this group (93 Å^2 with a modeled occupancy of 0.5) is very high in comparison with the equivalent phosphate groups in other LSs, which is also in agreement with a weaker interaction with the phosphate ion.

Catalytic activity measurement of *Brucella* spp. RibH2 is in agreement with these observations. Table 4 summarizes the kinetic parameters for this enzyme in comparison to the icosahedral *B. subtilis* and the pentameric *S. cerevisiae* LS (V.Z. *et al.*, unpublished results).[27,28] There is no major difference with respect to the kinetic constant K_M for the 5-amino-6-(D-ribitylamino)-2,4(1*H*,3*H*)-pyrimidinedione substrate **1**. On the other hand, K_M for substrate **2** shows noteworthy differences for *Brucella* spp. As stated above, the absence of a positively charged group close to the phosphate-binding site leads to weaker binding of this substrate, giving rise to a K_M of about two orders of magnitude higher than that observed in the pentameric and icosahedral enzymes. Previous studies on *B. subtilis* LS demonstrated the importance of the guanidinium group of Arg127 in anchoring the phosphate ion.[11,28] It has been
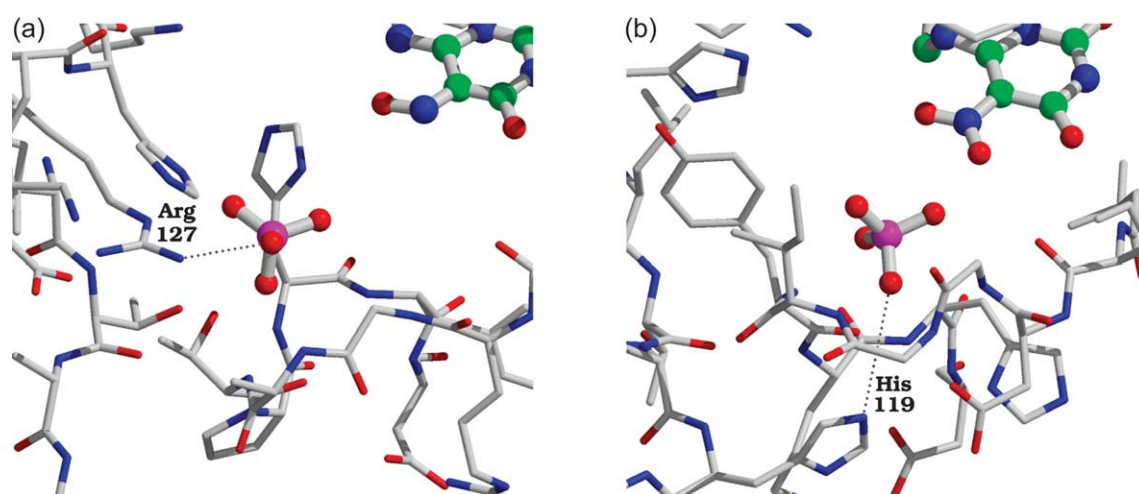

Figure 11. Divergence in the phosphate-binding site of different LS. (a) Icosahedral *A. aeolicus* lumazine synthase complexed with the substrate analogue inhibitor 5-nitroso-6-(D-ribitylamino)-2,4(1*H*,3*H*)-pyrimidinedione. (b) Decameric *Brucella* spp. RibH2-NRP. Electrostatic interactions between the phosphate group and the charged residues are shown as dotted lines.

Table 4. Enzymatic parameters of *Brucella* spp. RibH2 in comparison with a pentameric and an icosahedral LS

Enzyme	K_M **1** (μM)	K_M **2** (μM)	k_{cat} (s^{-1})	k_{cat}/K_M **1** (M^{-1} s^{-1})	k_{cat}/K_M **2** (M^{-1} s^{-1})
Brucella spp. RibH2	10	4000	0.006	600	1.5
B. subtilis LS	8.6	55	0.056	6500	1020
S. cerevisiae LS	4.0	90	0.080	20,000	880

found that mutation of this residue to non-ionizable amino acids such as Ala, Leu, Ser and Thr results in a complete inactivation of the enzyme, whereas the more conservative Arg127His mutant retains approximately half of the catalytic activity. Although the *Brucella* spp. enzyme lacks this arginine residue, the presence of His119 due to the different quaternary arrangement leads to a residual LS activity. The turnover number k_{cat} for RibH2 is reduced approximately ten times in comparison with other LS, leading to catalytic efficiencies (k_{cat}/K_M) of about three orders of magnitude smaller for the substrate **2** and more than one order of magnitude smaller for the substrate **1**.

The extremely high K_M value for substrate **2** (4 mM) and the evident lower catalytic activity of *Brucella* spp. RibH2, in comparison with other known LS, prompts us to postulate that the true function of this enzyme is not associated with the primary riboflavin biosynthetic pathway. This hypothesis is further enhanced with the recent discovery of a protein in the *Brucella* spp. genome (RibH1) for which preliminary catalytic parameters resemble those of the pentameric and icosahedral LS (V.Z. *et al.*, unpublished results). This makes RibH1 a more likely candidate for primary ribo-flavin synthesis.[29–31] Data mining studies have shown that the RibH1 gene is part of the Rib operon, which encodes for all the enzymes of riboflavin biosynthesis.[32] In contrast, RibH2 has evolved to a different role in the cell, although conserving a residual LS activity due to the relatively comparable architecture of its active site with respect to other LS.

Conclusions

Here, we explain, from a structural point of view, the differences in the enzymatic properties of *Brucella* spp. RibH2 that make this protein catalyze the penultimate step in riboflavin biosynthesis less effectively than other LSs. We find a strong relationship between quaternary structure and function in this enzyme. The insertion of a few residues in a specific region of the chain leads to a novel quaternary arrangement that affects the architecture of the active site, especially at the binding site of the substrate **2**. We also show that substrate **1** is recognized in a way similar to that in other LSs, evidence for a high degree of conservation of this region of the active site among species.

The residual LS activity of RibH2 and the presence of a second enzyme (RibH1) that catalyzes this reaction more efficiently are strong evidence that the actual function of RibH2 is not related to the normal riboflavin pathway. The present results can explain how the evolved quaternary change has affected the enzymatic properties of this protein. As such, the significant influence of pH on the RibH2 structure, as well as the redox properties of riboflavin and 6,7-dimethyl-8-ribityllumazine, which bind to this enzyme, could be key elements that lead to the precise identification of the function of RibH2 in the pathogen *Brucella* spp.

Materials and Methods

Materials

NRP and 6,7-dimethyl-8-ribityllumazine were kindly provided by Dr Adelbert Bacher, Technische Universität München, Germany. Riboflavin was purchased from Sigma-Aldrich (St. Louis, MO).

Protein cloning and expression

The RibH2-encoding gene was cloned into the expression plasmid pET11b (Novagen, Madison, WI) as described.[21] This construction was used to transform *Escherichia coli* BL21(DE3) competent cells (Stratagene, La Jolla, CA). Recombinant colonies were grown at 37 °C to an A_{600} of 1.0 in LB medium containing 100 μg/ml of ampicillin with agitation (300 rpm). A portion (5 ml) of this preparation was diluted to 500 ml and grown again until $A_{600}=1.0$. At this point, the culture was induced by the addition of 1 mM IPTG and incubated for 4 h at 37 °C with agitation (300 rpm), leading to a high yield of RibH2 as inclusion bodies. The bacteria were centrifuged at 15,000g for 20 min at 4 °C and stored at −20 °C.

Protein purification

The bacterial pellet was suspended and sonicated in 50 mM Tris (pH 8.0), 5 mM EDTA, 1% (v/v) Triton X-100. Inclusion bodies were washed with solution lacking Triton X-100 and then solubilized at room temperature in 50 mM Tris (pH 8.0), 5 mM EDTA, 8 M urea, overnight with agitation. The material was dialyzed extensively against PBS containing 1 mM DTT with several changes of buffer, in order to achieve protein refolding. This preparation was purified by anion-exchange chromato-graphy in an FPLC apparatus using a Mono-Q column (Amersham Biosciences, Uppsala, Sweden) equilibrated in buffer A (50 mM Tris (pH 8.5), 1 mM DTT). The fractions were eluted using a linear gradient of 0–1 M sodium chloride. The protein was then amidinated with 25 mM iodoacetamide at room temperature for 1 h in the dark in order to block its single free cysteine residue (Cys7). The protein was further purified by size-exclusion chromatography in a Superdex 200 column with isocratic

elution in PBS. RibH2 was finally dialyzed in crystallization buffer (10 mM sodium/potassium phosphate (pH 5.5), 25 mM NaCl), concentrated by centrifugation to ~10 mg/ml with Centricon YM-10 concentrators (Millipore, Billerica, MA) and stored at −20 °C.

Crystallization

Crystals were obtained by means of the hanging-drop, vapor-diffusion method at room temperature. RibH2 and NRP were cocrystallized with 0.1 M Mes (pH 6.5), 30% (w/v) PEG 400, 0.1 M sodium acetate, with a final mother liquor pH of 6.3. A mixture of 1 μl of protein stock and 1 μl of the precipitant solution, in the presence of a fourfold molar excess of the substrate analogue inhibitor NRP, were equilibrated against precipitant. Diamond-shaped crystals of about 0.30 mm×0.20 mm×0.20 mm appeared after three days. Crystallization of RibH2-ORTH yielded long triangular prisms of about 0.30 mm×0.05 mm× 0.05 mm after several weeks when crystallized against 0.1 M Mes (pH 6.3), 1.3 M ammonium sulfate, having a final pH of 6.5.

Data collection and processing

Preliminary X-ray diffraction data were collected with our in-house X-ray source, a Bruker M18XH6 MAC Science rotating anode generator and a Siemens X-1000 multiwire area detector. The final datasets were obtained at the D03B Protein Crystallography Beamline at the Laboratório Nacional de Luz Síncrotron, Campinas, Brazil[33] with λ=1.427 Å and using an MarCCD detector (Mar USA, Evanston, IL). RibH2-ORTH crystals were

soaked in 25% (v/v) glycerol in mother liquor and flash-cooled in a 100 K nitrogen stream. RibH2-NRP crystals could be cooled directly without any additional cryo-protectant due to the high content of PEG 400 in their mother liquor. Frames were collected in Time mode with 1° oscillation each. Only one crystal was used for the collection of each dataset. Data indexing, integration, scaling and reduction were performed with the programs MOSFLM, Scala and Truncate from the CCP4 package.[34] RibH2-NRP crystals diffracted to a maximum resolution of 2.90 Å and belong to the trigonal space group $P3_121$, with one pentamer in the asymmetric unit and a high solvent content (70.8%, v/v). RibH2-ORTH best crystals diffracted to 3.05 Å and belong to the orthorhombic space group $P2_12_12_1$, with a full decamer in the asymmetric unit. A total of 5% of the measured reflections were flagged for cross-validation. Full details of data collection statistics are shown in Table 5.

Structure solution

Both structures presented here were solved by the molecular replacement method with the program AMoRe,[35] using the pentameric model of the previously determined *Brucella* spp. RibH2 structure (RibH2-RHO; PDB entry 1DI0)[25] as search model, with some conflicting residues mutated to alanine in order to reduce model bias. Due to the minimal differences between the search model and the unknown structures, phasing was straightforward. In RibH2-NRP, a total of five solutions were obtained in the asymmetric unit, rotated 72° from each other, due to the pentameric assembly of this enzyme. Despite the fact that we found only one pentamer in the asymmetric unit, the actual decameric quaternary arrangement of this protein[24] could be recovered easily by means of the symmetry operators of the $P3_121$ space group. In contrast, RibH2-ORTH crystallized with two pentamers in the asymmetric unit, thus allowing us to work directly with the decameric motif along the whole structure determination process.

Model building and refinement

The best molecular replacement solutions of both structures were subjected to rigid-body refinement using the fitting function of AMoRe[35] and checked for consistent packing between neighboring molecules in the crystal. At this point, the RibH2-NRP structure showed an R-factor of 0.439. The coordinates for this model were entered in CNS[36] for a cycle of positional and B-factor refinement, decreasing its R-factor to 0.315. Single and double difference Fourier maps calculated at this stage showed a strong and well-defined electronic density near each of the five topologically equivalent active sites of the enzyme, which correspond to the bound substrate analogue inhibitor NRP. Coordinates of this molecule were obtained from the PDB entry 1KYY (LS from *S. pombe* bound to the same ligand)[19] and fit into the density using the program O.[37] Model building also included several side-chain shifts, especially in residues involved in crystallographic contacts between pentamers, and rebuilding of some residues that were previously modeled as alanine. Refinement was carried out using the maximum likelihood algorithm and cycles of simulated annealing. Reflections with $F < 2\sigma$ were excluded from the process. Topology and parameter libraries for the ligand were obtained from the HIC-Up database.[38] During the final stages of refinement, a few solvent molecules and

Table 5. X-ray data collection parameters and processing statistics for RibH2-NRP and RibH2-ORTH

	RibH2-NRP	RibH2-ORTH
Data collection		
Number of frames	180	111
Oscillation step (deg.)	1	1
Crystal-to-detector distance (mm)	110	120
Exposure per frame (s)	90	120
Indexing and scaling		
Cell parameters (Å)		
a	126.32	116.55
b	126.32	120.24
c	165.67	159.37
Cell angles (deg.)		
α	90	90
β	90	90
γ	120	90
Space group	$P3_121$	$P2_12_12_1$
Resolution limit (Å)	2.90	3.05
Total reflections	367,635	192,472
Unique reflections	34,483	43,004
Multiplicity[a]	10.7 (10.6)	4.5 (4.3)
I/σ	6.6 (2.4)	5.8 (2.2)
R_{merge} (%)[b]	9.3 (30.7)	12.2 (33.1)
Completeness (%)	100.0 (100.0)	99.2 (98.8)
Pentamers/asymmetric unit	1	2
Solvent content (%)	70.8	60.0
Matthews coefficient (Å³/Da)	4.2	3.1
B-factor (Wilson plot, Å²)	63.4	49.6

[a] Values in parentheses correspond to the highest resolution shell: RibH2-NRP: 3.06–2.90 Å, RibH2-ORTH: 3.21–3.05 Å.
[b] $R_{merge} = [\sum_i |I_i - \langle I \rangle| / \sum_i I_i]$.

phosphate ions were introduced manually due to the moderate resolution of this structure. We obtained a final model with $R = 0.217$ and $R_{\text{free}} = 0.254$, with good geometry. RibH2-ORTH was refined using the same programs and procedures, yielding a final model with $R = 0.199$ and $R_{\text{free}} = 0.256$. Both structures were refined without NCS restraints during the whole process. Further details of refinement statistics are shown in Table 1.

Determination of kinetic and thermodynamic parameters in solution

Enzymatic activity, as well as K_M and K_D parameters, were assayed according to published procedures.[10,28,39] Briefly, fluorescence titration was performed to obtain K_D from 6,7-dimethyl-8-ribityllumazine ($\lambda_{\text{exc}} = 408$ nm, $\lambda_{\text{emis}} = 487$ nm) and riboflavin ($\lambda_{\text{exc}} = 445$ nm, $\lambda_{\text{emis}} = 516$ nm). For this purpose, a total of 100 μl of ligand solution was added in steps of 5 μl to 1 ml of 1 μM RibH2 solution in 50 mM potassium phosphate (pH 7.0), and fluorescence emission was measured after each aliquot with a Jasco FP-770 spectrofluorometer (Jasco Inc., Easton, MD) at 25 °C. Control experiments were performed with 1 ml of 50 mM potassium phosphate (pH 7.0).

K_D for the substrate analogue inhibitor NRP was calculated in a different manner, taking into account that its binding affects the environment of Trp22 and quenches its fluorescence. For this measurement, different concentrations of NRP were added to a 1.4 μM RibH2 solution in 50 mM potassium phosphate (pH 6.5). Then, a suitable fitting of the measured fluorescence in function of NRP concentration ($\lambda_{\text{exc}} = 280$ nm, $\lambda_{\text{emis}} = 350$ nm) allowed determination of K_D.

Finally, in order to obtain k_{cat} and K_M, a series of solutions containing RibH2, substrates **1** and **2**, 100 mM potassium phosphate (pH 7.0) and 5 mM EDTA were prepared. The generation of 6,7-dimethyl-8-ribityllumazine was monitored by measuring the absorbance at 410 nm and 37 °C. In all cases, reaction mixtures lacking the enzyme were used to correct the measured values due to the appreciable non-enzymatic generation of product.[40]

Graphical representation and analysis of the models

The quality of the models was assessed using the programs PROCHECK[41] and SFCHECK.[42] Superpositions and r.m.s.d. calculations were done with the Protein Structure Comparison Service SSM at the European Bioinformatics Institute.[43] Figures were created with O,[37] MOLSCRIPT,[44] Raster3D,[45] Chimera[46] and ChemDraw (CambridgeSoft, Cambridge, MA).

Protein Data Bank accession codes

Atomic coordinates and structure factors have been deposited in the RCSB Protein Data Bank. The accession codes of the protein structures presented here are 1T13 for RibH2-NRP and 1XN1 for RibH2-ORTH.

Acknowledgements

References

1. Kearney, E. B., Goldenberg, J., Lipsick, J. & Perl, M. (1979). Flavokinase and FAD synthetase from *Bacillus subtilis* specific for reduced flavins. *J. Biol. Chem.* **254**, 9551–9557.

2. Oltmanns, O., Bacher, A., Lingens, F. & Zimmermann, F. K. (1969). Biochemical and genetic classification of riboflavine deficient mutants of *Saccharomyces cerevisiae*. *Mol. Gen. Genet.* **105**, 306–313.

3. Shavlovsky, G. M., Teslyar, G. E. & Strugovshchikova, L. P. (1982). Regulation of flavogenesis in riboflavin dependent *Escherichia coli* mutants. *Mikrobiologiya*, **51**, 986–992.

4. Bacher, A., Fischer, M., Kis, K., Kugelbrey, K., Mortl, S., Scheuring, J. *et al.* (1996). Biosynthesis of riboflavin: structure and mechanism of lumazine synthase. *Biochem. Soc. Trans.* **24**, 89–94.

5. Neuberger, G. & Bacher, A. (1986). Biosynthesis of riboflavin Enzymatic formation of 6,7-dimethyl-8-ribityllumazine by heavy riboflavin synthase from *Bacillus subtilis*. *Biochem. Biophys. Res. Commun.* **139**, 1111–1116.

6. Volk, R. & Bacher, A. (1988). Biosynthesis of riboflavin. The structure of the 4-carbon precursor. *J. Am. Chem. Soc.* **110**, 3651–3653.

7. Volk, R. & Bacher, A. (1990). Studies on the 4-carbon precursor in the biosynthesis of riboflavin. Purification and properties of L-3,4-dihydroxy-2-butanone-4-phosphate synthase. *J. Biol. Chem.* **265**, 19479–19485.

8. Bacher, A. & Ladenstein, R. (1991). The lumazine synthase/riboflavin synthase complex of *Bacillus subtilis*. In *Chemistry and Biochemistry of Flavoproteins* (Müller, F., ed.), vol. 1, pp. 215–259, CRC Press, Boca Raton, FL.

9. Bacher, A., Eberhardt, S. & Richter, G. (1996). Biosynthesis of riboflavin. In Escherichia *and* Salmonella (Neidhardt, F. C., Ingraham, J. L., Low, K. B., Magasanik, B., Schaechter, M. & Umbarger, H. E., eds), vol. 1, pp. 657–664, American Society for Microbiology, Washington, DC.

10. Kis, K., Volk, R. & Bacher, A. (1995). Biosynthesis of riboflavin. Studies on the reaction mechanism of 6,7-dimethyl-8-ribityllumazine synthase. *Biochemistry*, **34**, 2883–2892.

11. Zhang, X., Meining, W., Cushman, M., Haase, I., Fischer, M., Bacher, A. & Ladenstein, R. (2003). A structure-based model of the reaction catalyzed by lumazine synthase from *Aquifex aeolicus*. *J. Mol. Biol.* **328**, 167–182.

12. Schramek, N., Haase, I., Fischer, M. & Bacher, A. (2003). Biosynthesis of riboflavin. Single turnover kinetic analysis of 6,7-dimethyl-8-ribityllumazine synthase. *J. Am. Chem. Soc.* **125**, 4460–4466 doi: 10.1021/ja028226k.

13. Persson, K., Schneider, G., Jordan, D. B., Viitanen, P. V. & Sandalova, T. (1999). Crystal structure analysis of a pentameric fungal and an icosahedral plant lumazine synthase reveals the structural basis for differences in assembly. *Protein Sci.* **8**, 2355–2365.

14. Ladenstein, R., Schneider, M., Huber, R., Bartunik, H. D., Wilson, K., Schott, K. & Bacher, A. (1988).

Heavy riboflavin synthase from *Bacillus subtilis*. Crystal structure analysis of the icosahedral β60 capsid at 3.3 Å resolution. *J. Mol. Biol.* **203**, 1045–1070.

15. Ladenstein, R., Ritsert, K., Huber, R., Richter, G. & Bacher, A. (1994). The lumazine synthase/riboflavin synthase complex of *Bacillus subtilis*. X-ray structure analysis of hollow reconstituted beta-subunit capsids. *Eur. J. Biochem.* **223**, 1007–1017.

16. Ritsert, K., Huber, R., Turk, D., Ladenstein, R., Schmidt-Bäse, K. & Bacher, A. (1995). Studies on the lumazine synthase/riboflavin synthase complex of *Bacillus subtilis*: crystal structure analysis of reconstituted, icosahedral beta-subunit capsids with bound substrate analogue inhibitor at 2.4 Å resolution. *J. Mol. Biol.* **253**, 151–167.

17. Zhang, X., Meining, W., Fischer, M., Bacher, A. & Ladenstein, R. (2001). X-ray structure analysis and crystallographic refinement of lumazine synthase from the hyperthermophile *Aquifex aeolicus* at 1.6 Å resolution: determinants of thermostability revealed from structural comparisons. *J. Mol. Biol.* **306**, 1099–1114.

18. Morgunova, E., Meining, W., Illarionov, B., Haase, I., Jin, G., Bacher, A. *et al.* (2005). Crystal structure of lumazine synthase from *Mycobacterium tuberculosis* as a target for rational drug design: binding mode of a new class of purinetrione inhibitors. *Biochemistry,* **44**, 2746–2758.

19. Gerhardt, S., Haase, I., Steinbacher, S., Kaiser, J. T., Cushman, M., Bacher, A. *et al.* (2002). The structural basis of riboflavin binding to *Schizosaccharomyces pombe* 6,7-dimethyl-8-ribityllumazine synthase. *J. Mol. Biol.* **318**, 1317–1329.

20. Meining, W., Mörtl, S., Fischer, M., Cushman, M., Bacher, A. & Ladenstein, R. (2000). The atomic structure of pentameric lumazine synthase from *Saccharomyces cerevisiae* at 1.85 Å resolution reveals the binding mode of a phosphonate intermediate analogue. *J. Mol. Biol.* **299**, 181–197.

21. Goldbaum, F. A., Velikovsky, C. A., Baldi, P. C., Mörtl, S., Bacher, A. & Fossati, C. A. (1999). The 18-kDa cytoplasmic protein of Brucella species-an antigen useful for diagnosis is a lumazine synthase. *J. Med. Microbiol.* **48**, 833–839.

22. Goldbaum, F. A., Leoni, J., Wallach, J. C. & Fossati, C. A. (1993). Characterization of an 18-kilodalton *Brucella* cytoplasmic protein which appears to be a serological marker of active infection of both human and bovine brucellosis. *J. Clin. Microbiol.* **31**, 2141–2145.

23. Baldi, P. C., Giambartolomei, G. H., Goldbaum, F. A., Abdon, L. F., Velikovsky, C. A., Kittelberger, R. & Fossati, C. A. (1996). Humoral immune response against lipopolysaccharide and cytoplasmic proteins of *Brucella abortus* in cattle vaccinated with *B. abortus* S19 or experimentally infected with *Yersinia enterocolitica* serotype 0:9. *Clin. Diagn. Lab. Immunol.* **3**, 472–476.

24. Zylberman, V., Craig, P. O., Klinke, S., Braden, B. C., Cauerhff, A. & Goldbaum, F. A. (2004). High order quaternary arrangement confers increased structural stability to *Brucella* sp. lumazine synthase. *J. Biol. Chem.* **279**, 8093–8101.

25. Braden, B. C., Velikovsky, C. A., Cauerhff, A. A., Polikarpov, I. & Goldbaum, F. A. (2000). Divergence in macromolecular assembly: X-ray crystallographic structure analysis of lumazine synthase from *Brucella abortus*. *J. Mol. Biol.* **297**, 1031–1036.

26. Laplagne, D. A., Zylberman, V., Ainciart, N., Steward, M. W., Sciutto, E., Fossati, C. A. & Goldbaum, F. A. (2004). Engineering of a polymeric bacterial protein as a scaffold for the multiple display of peptides. *Proteins: Struct. Funct. Genet.* **57**, 820–828.

27. Mörtl, S., Fischer, M., Richter, G., Tack, J., Weinkauf, S. & Bacher, A. (1996). Biosynthesis of riboflavin. Lumazine synthase of *Escherichia coli*. *J. Biol. Chem.* **271**, 33201–33207.

28. Fischer, M., Haase, I., Kis, K., Meining, W., Ladenstein, R., Cushman, M. *et al.* (2003). Enzyme catalysis *via* control of activation entropy: site-directed mutagenesis of 6,7-dimethyl-8-ribityllumazine synthase. *J. Mol. Biol.* **326**, 783–793.

29. DelVecchio, V. G., Kapatral, V., Redkar, R. J., Patra, G., Mujer, C., Los, T. *et al.* (2002). The genome sequence of the facultative intracellular pathogen *Brucella melitensis*. *Proc. Natl Acad. Sci. USA*, **99**, 443–448.

30. Paulsen, I. T., Seshadri, R., Nelson, K. E., Eisen, J. A., Heidelberg, J. F., Read, T. D. *et al.* (2002). The *Brucella suis* genome reveals fundamental similarities between animal and plant pathogens and symbionts. *Proc. Natl Acad. Sci. USA*, **99**, 13148–13153.

31. Halling, S. M., Peterson-Burch, B. D., Bricker, B. J., Zuerner, R. L., Qing, Z., Li, L. L. *et al.* (2005). Completion of the genome sequence of *Brucella abortus* and comparison to the highly similar genomes of *Brucella melitensis* and *Brucella suis*. *J. Bacteriol.* **187**, 2715–2726.

32. Vitreschak, A. G., Rodionov, D. A., Mironov, A. A. & Gelfand, M. S. (2002). Regulation of riboflavin biosynthesis and transport genes in bacteria by transcriptional and translational attenuation. *Nucl. Acids Res.* **30**, 3141–3151.

33. Polikarpov, I., Oliva, G., Castellano, E. E., Garratt, R. C., Arruda, P., Leite, A. & Craievich, A. (1998). The protein crystallography beamline at LNLS, the Brazilian National Synchrotron Light Source. *Nucl. Instrum. Meth. Phys. Res. A*, **405**, 159–164.

34. Collaborative Computational Project Number 4 (1994). The CCP4 suite: programs for protein crystallography. *Acta Crystallog. sect. D*, **50**, 760–763.

35. Navaza, J. A. C. (1994). AMoRe: an automated package for molecular replacement. *Acta Crystallog. sect. A*, **50**, 157–163.

36. Brunger, A. T., Adams, P. D., Clore, G. M., Delano, W. L., Gros, P., Grosse-Kunstleve, R. W. *et al.* (1998). Crystallography & NMR system (CNS): a new software system for macromolecular structure determination. *Acta Crystallog. sect. D*, **54**, 905–921.

37. Jones, T. A., Zou, J. Y., Cowan, S. W. & Kjeldgaard, M. (1991). Improved methods for the building of protein models in electron density maps and the location of errors in these models. *Acta Crystallog. sect. A*, **47**, 110–119.

38. Kleywegt, G. J. & Jones, T. A. (1998). Databases in protein crystallography. *Acta Crystallog. sect. D*, **54**, 1119–1131.

39. Fischer, M., Haase, I., Feicht, R., Richter, G., Gerhardt, S., Changeux, J. P., Huber, R. & Bacher, A. (2002). Biosynthesis of riboflavin: 6,7-dimethyl-8-ribityllumazine synthase of *Schizosaccharomyces pombe*. *Eur. J. Biochem.* **269**, 519–526.

40. Kis, K., Kugelbrey, K. & Bacher, A. (2001). Biosynthesis of riboflavin. The reaction catalyzed by 6,7-dimethyl-8-ribityllumazine synthase can proceed without enzymatic catalysis under physiological conditions. *J. Org. Chem.* **66**, 2555–2559.

41. Laskowski, R. A., MacArthur, M. W., Moss, D. S. &

Thornton, J. M. (1993). PROCHECK: a program to check the stereochemical quality of protein structures. *J. Appl. Crystallog.* **26**, 283–291.

42. Vagin, A. A., Richelle, J. & Wodak, S. J. (1999). SFCHECK: a unified set of procedure for evaluating the quality of macromolecular structure-factor data and their agreement with atomic model. *Acta Crystallog. sect. D*, **55**, 191–205.

43. Krissinel, E. & Henrick, K. (2004). Secondary-structure matching (SSM), a new tool for fast protein structure alignment in three dimensions. *Acta Crystallog. sect. D*, **60**, 2256–2268.

44. Kraulis, P. J. (1991). MOLSCRIPT: a program to produce both detailed and schematic plots of protein structures. *J. Appl. Crystallog.* **24**, 946–950.

45. Merritt, E. A. & Bacon, D. J. (1997). Raster3D: photorealistic molecular graphics. *Methods Enzymol.* **277**, 505–524.

46. Pettersen, E. F., Goddard, T. D., Huang, C. C., Couch, G. S., Greenblatt, D. M., Meng, E. C. & Ferrin, T. E. (2004). UCSF Chimera - a visualization system for exploratory research and analysis. *J. Comput. Chem.* **25**, 1605–1612.